Available online at www.sciencedirect.com
ScienceDirect
Journal of Power Sources 162 (2006) 215–227
JOURNAL OF POWER SOURCES
www.elsevier.com/locate/jpowsour

Control-oriented modelling and experimental study of the transient response of a high-temperature polymer fuel cell

Federico Zenith [a,*], Frode Seland [b], Ole Edvard Kongstein [b], Børre Børresen [b], Reidar Tunold [b], Sigurd Skogestad [a]

[a] *Department of Chemical Engineering, Norwegian University of Science and Technology, Sem Sælands veg 4, 7491 Trondheim, Norway*
[b] *Department of Materials Science and Engineering, Norwegian University of Science and Technology, Sem Sælands veg 12, 7491 Trondheim, Norway*

Received 27 September 2005; received in revised form 16 May 2006; accepted 9 June 2006
Available online 31 July 2006

Abstract

Fuel-cell dynamics have been investigated with a variable-resistance board applied to a high-temperature polymer fuel cell, operating on pure oxygen and hydrogen at atmospheric pressure and about 150 °C. A particular pattern has been identified in the voltage–current density diagram. A model has been developed, using a characteristic equation to represent the external circuit as a resistive load, possibly nonlinear and time-varying, rather than assuming the current density to be an independent variable. The model successfully explains the shape of the transient current–voltage paths, including the different time constants observed when reversing a transient.

Keywords: Fuel cell; Polybenzimidazole; Model; Dynamics; Control

1. Introduction

The interest in fuel cells is increasing because of the role they might play in many power-delivering utilities in various scales, with environmental benefits and increased efficiency. Many research papers are published, but most of them assume steady-state conditions for the cell.

Recently, interest has increased also for the dynamic behaviour of fuel cells, as a topic in its own merit and as a prerequisite for control analysis and controller design. However, many models provided in the literature [1–5] were not intended for control studies, and in that context they are often "flawed" because they consider *current density* as an input to the system. This is unrealistic from a process-control perspective, because in reality the current is determined by the characteristics of the fuel cell and of its external load [6]. For example, it has been shown by Weydahl et al. [7] and Rao and Rengaswamy [8] that the current does not change stepwise during specific transients, but instead follows a certain pattern, which may be described by a step change followed by what appears to be an exponential relaxation. A better approach for models with realistic inputs is therefore using the load's characteristic as an input instead.

Conventional polymer electrolyte membrane (PEM) fuel cells employ an electrolyte that relies on liquid water to facilitate protonic conduction, and operate at a temperature ranging from 50 to 90 °C, unless pressurised. Careful control of the heat and mass balances is necessary in order to avoid drying out the electrolyte membrane or flooding the gas-diffusion electrodes.

Polybenzimidazole (PBI) represents a new generation of thermally resistant polymer electrolyte membranes with a reported glass transition temperature of 420 °C [9]. The conductivity of PBI in its pure state is very low, about 10^{-12} S cm^{-1} [10,11]. Several studies of the conductivity in acid-doped PBI-membranes for fuel cells have been published in the last few years [12–16]. The most frequently used dopant is phosphoric acid, as first introduced by Wainright et al. [17]. Phosphoric acid-doped PBI fuel cells allow for an operating temperature as high as 200 °C. He et al. [15] found the conductivity of PBI to be

* Corresponding author. Tel.: +47 73 56 39 42; fax: +47 73 59 40 80.
E-mail addresses: zenith@chemeng.ntnu.no (F. Zenith), frodesel@material.ntnu.no (F. Seland), oleko@material.ntnu.no (O.E. Kongstein), btbo@statoil.com (B. Børresen), Reidar.Tunold@material.nt.ntnu.no (R. Tunold), skoge@chemeng.ntnu.no (S. Skogestad)..

0378-7753/$ – see front matter © 2006 Elsevier B.V. All rights reserved.
doi:10.1016/j.jpowsour.2006.06.022

Nomenclature

a	activity
A	electrode area (m^2)
C	specific capacitance ($F\,m^{-2}$)
D	diffusivity coefficient ($m^2\,s^{-1}$)
E^{rev}	reversible voltage (V)
F	Faraday's constant ($C\,mol^{-1}$)
Δg_f	specific Gibbs free energy of formation ($J\,mol^{-1}$)
i	circuit current density ($A\,m^{-2}$)
i_c	crossover current density ($A\,m^{-2}$)
i_L	mass-transfer-limiting current density ($A\,m^{-2}$)
i_r	reaction current density ($A\,m^{-2}$)
i_0	exchange current density ($A\,m^{-2}$)
I	current (A)
k	reaction rate constant ($mol\,m^{-2}\,s^{-1}$)
L	thickness of the diffusion layer (m)
n	number of exchanged electrons
N	molar flux ($mol\,m^{-2}\,s^{-1}$)
p	pressure (Pa)
r	specific resistance ($\Omega\,m^2$)
R	gas constant ($J\,mol^{-1}K^{-1}$)
t	time (s)
T	temperature (K)
V	voltage (V)
x	distance from the reaction surface (m)

Greek letters

α	charge-transfer coefficient
ε	porosity
η	activation overvoltage (V)
λ	equivalent thickness of the diffusion layer (m)
ξ	tortuosity
τ	time constant (s)

$6.8 \times 10^{-2}\,S\,cm^{-1}$ at 200 °C with a H_3PO_4 doping level of 5.6 (mole number of H_3PO_4 per repeat unit of PBI) and 5% relative humidity.

High-temperature PEM fuel cells based on phosphoric acid-doped PBI-membranes and operating up to 200 °C have several advantages over conventional PEM fuel cells working at temperatures lower than 100 °C. The increased temperature improves the reaction kinetics in the sluggish phosphoric acid environment, simplifies the heat and mass transport management and leads to an increased tolerance towards carbon monoxide, which is of major importance for platinum-based catalysts. Li et al. [18] demonstrated the enhanced CO tolerance in a PBI fuel cell at elevated temperatures and found a CO tolerance of 3% CO in hydrogen at current densities up to $0.8\,A\,cm^{-2}$ at 200 °C. This significantly simplifies the pre-treatment of the fuel and makes the PBI fuel cells a viable alternative to the low-temperature PEM fuel cells.

Currently, there are not many papers about control of fuel cells. For example, as of March 2006, only two articles about fuel cells has been published in the Journal of Process Control [19,20]. However, sections about control of fuel cells can be found in papers about dynamics of fuel cells, or outside the process-control literature. For instance, Iqbal [21] devised a control system for a fuel cell connected to a wind power plant; however, since he used the Ziegler-Nichols PID-setting rules, his resulting controller was too aggressive, and did not properly reject disturbances, especially the variation in wind speed. An attempt to devise a simple control system for a PBI fuel cell is present in a MSc thesis by Johansen [22], but the results were not encouraging; the use of a simple proportional controller was shown to deliver insufficient tracking performance. Pukrushpan, in his doctoral thesis [23], concentrated on the dynamics and control of the gas flow systems, including natural-gas reformers, anode humidifiers, and compressors; however, based on previous claims by Guzzella [24], he claimed that the time constant of the electrochemical transient was in the order of magnitude of 10^{-9} s,[1] which is contradicted by laboratory evidence; the electrochemical transient is in the range of 10^{-3} to 10 s for alkaline [7,25] fuel cells, and in the range of 10–100 s for direct-methanol fuel cells [26]. As it will be shown later, PBI fuel cells have transients typically lasting between 10^{-1} and 1 s.

Understanding the dynamic behaviour of a PBI fuel cell will be useful in developing efficient control algorithms, which are a necessary step before applications using this type of fuel cells can be marketed. Since PBI fuel cells require temperatures higher than the environment's, the most likely applications would be in the higher range of power ratings, such as the automotive and power-generation sectors. The analysis presented in this paper may be adapted to other types of fuel cells, highlighting similarities and differences among different types of fuel cells.

The objective of this paper is to show the development of a dynamic model using the external circuit's characteristic as an input, and how this model is able to explain experimental results observed on a high-temperature polymer (PBI-based) fuel cell. The first data confirming the model came actually from experiments already done on alkaline fuel cells [7], as there are no significant differences between this model and a model specifically designed for alkaline fuel cells in the data range where the experiments were carried out. The measurements were later repeated on PBI-based fuel cells, with similar results; however, in the PBI fuel cell, there were also superimposing transients that were found to be much slower.

2. Experimental setup and procedure

2.1. Experimental setup

Experiments were carried out on a PBI membrane-electrode assembly, prepared in-house at Department of Materials Science

[1] In actuality Pukrushpan claimed 10^{-19} s in his thesis, but this is most likely due to a typing error.

and Engineering of NTNU, in order to determine the transient response of the cell to a variable load. The laboratory setup is sketched in Fig. 1. This project is part of the FURIM project in the European 6th Framework Programme, contract number SES6-CT-2004-502782.

The load itself was assembled as a variable-resistance board, with two resistances in parallel; in series with one of these resistances, a switch could be opened and closed manually, changing the total resistance of the circuit. The value of the resistances could be selected manually from the 11 positions of two corresponding knobs. The resistance board was recently developed by Helge Weydahl in a related study [7].

The cell could be kept at a given temperature by a custom-made external electric heater with a feedback control loop, consisting of a thermocouple and an electronic control unit (West® 6400 1/16 DIN profile controller). It should be noted that, whereas the laboratory setup needed make-up heat because of its small size, an application will probably need cooling instead, since the reaction heat will be sufficient to maintain its temperature.

The fuel cell ran on 99.5% hydrogen and 99.5% oxygen at atmospheric pressure. Oxygen was fed the cell directly, whereas hydrogen was bubbled through a 37.5% H_3PO_4 solution, in order to make up for any loss of phosphoric acid in the cell's membrane. Both exhaust streams were bubbled through distilled water, to provide a simple visual flow feedback. All streams were controlled with a flow-control unit by Hi-Tek®.

To acquire data, an Agilent® 34970A data-acquisition unit was used; the data was later exported from its interface program into Octave to produce plots.

A polarisation curve for the cell was measured using a Wenking® HP 96-20 potentiostat, whose voltage was set by a Wenking® MVS 98 Scan Generator. When measuring the polarisation curve, the potentiostat substituted the resistance board in Fig. 1.

2.2. Experimental procedure

Some general conditions were maintained in all tests:

- the cell was kept at a constant temperature of 150 °C;
- the oxygen flow was kept at 3.7 $cm^3\ s^{-1}$;
- the hydrogen flow was kept at 5.8 $cm^3\ s^{-1}$.

Since the data-acquisition unit could only make voltage measurements, the current through the circuit was always calculated from the voltage over a known, small resistance, integrated in the resistance board. The voltages measured by the data-acquisition unit and the times at which they were taken were the only measurement recorded. In order to have synchronous data for current and voltage, the time vectors associated with the current and voltage outputs were merged; each of the outputs was then linearly interpolated on the merged time vector.

For variable-resistance tests, the fuel cell was connected to the resistance board. After having reached steady-state in cell temperature and voltage, the data-acquisition unit was turned on and the board's switch was flipped. For consecutive tests, the switch could be flipped again after reaching a steady-state in voltage. The data could then be saved as a comma-separated value file. To obtain maximum detail, the data-acquisition unit was set to record data as fast as possible (about every 0.1 s).

To obtain a polarisation curve, the potentiostat was connected to the fuel cell instead of the resistance board. Because of the slow secondary dynamics, the measurement took about 18 h: the potentiostat cycled between 0.825 and 0 V at a sweep rate of 25 $\mu V\ s^{-1}$. In order to obtain a manageable number of data points, the data-acquisition unit was set to record data every 10 s.

The gas-diffusion electrodes were prepared by spraying a slurry of the relevant components with an airbrush (Badger No. 100G). First, a layer of carbon support was sprayed onto a carbon fiber paper (Toray, TGP-H-120), and subsequently a catalytic layer was sprayed on top of the support layer. The Pt catalyst loading was about 1 $mg\ cm^{-2}$ in total. The carbon

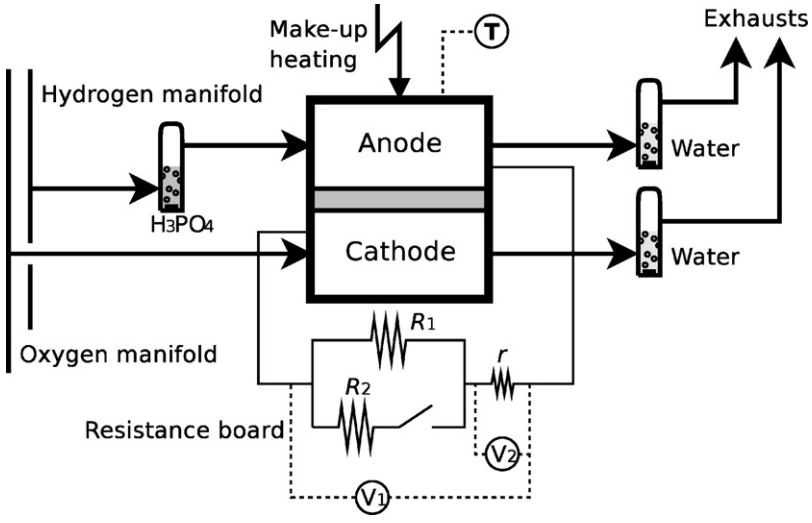

Fig. 1. The laboratory setup for the experiments. Resistances R_1 and R_2 can be set to 11 different values each. The fuel cell's voltage is measured by voltmeter V_1 and passed to the data-acquisition unit. Resistance r, known and fixed, is used to measure the current; its voltage is measured by V_2.

black (Vulcan XC-72) was provided by Cabot Corporation. The electrocatalyst, HiSPEC™ 8000 (50% Pt on Vulcan XC-72) was purchased from Johnson & Matthey, while the PBI-membrane was provided by the Technical University of Denmark (DTU) as a partner in the FURIM project, which is acknowledged. The membrane-electrode assembly (MEA) used in this work was made by hot-pressing a sandwich of PBI-membrane (4 cm×4 cm) and electrodes (2 cm×2 cm). A more detailed description of the MEA preparation is given elsewhere [27].

The MEA was tested in a commercially available fuel cell (ElectroChem, Inc.) with one reference electrode probe, double serpentine flow field and originally designed for low-temperature PEM fuel cells.

To determine whether the anodic overpotential could be neglected, it was measured by means of a dynamic hydrogen electrode in the same way as described by Küver et al. [28]. The dynamic hydrogen electrode current was supplied by a 1.6 V battery, to avoid any ground influence. The electrode potential was corrected for resistance by current interrupt. The anodic overpotential was measured with pure hydrogen at 150 °C.

2.3. Uncertainty analysis

The preparation of the membrane-electrode assembly is likely to have a major impact on the fuel cell's properties. Since PBI membranes are not commercially available in standard form, the variability encountered in reproducing the membrane may impair the reproducibility of the measurements reported in this paper. An effort was made to make the MEAs as reproducible as possible, as described in Seland et al. [27].

The influence of oxygen flow is going to depend also on the number and shape of the cathode channels. Precision in hydrogen flow, instead, has been found to be of little consequence. The performance of the flow controllers and of the temperature controller will also influence the resulting data, but this will result in systematic error rather than uncertainty.

The precision with which the board's resistances are known is going to have a direct influence the reliability of the measurements of current. Any unaccounted nonlinearities would also disturb the measurements.

Some transients had time constants in the same order of magnitude or even higher than the sampling rate. It is possible that some important points might be missed if a fast transient is not sampled with a sufficiently fast sensor, resulting in a significantly different shape of the transient measured.

3. Modelling and analysis

3.1. Objectives

The model presented here was originally conceived as a first step in a control analysis and synthesis for polybenzimidazole-based proton-exchange membrane fuel cells. This model has also been found suitable to describe the transient behaviour of alkaline fuel cells, when operating in conditions where the diffusion phenomena are not important [29]; it is expected that, except for diffusion-related issues, most results will hold also for Nafion®-based fuel cells as well.

For the purposes of process control, high modelling accuracy is usually not necessary: it is more common to produce a model that captures the essential behaviour of the system, and let a feedback loop even out the smaller inconsistencies as they were disturbances. It is more important to predict variations in the frequency range of interest than, for example, slow variations that can be taken care of by a PI controller.

The model tries therefore to reach an acceptable compromise between the number of parameters and accuracy. Many parameters have been lumped and some phenomena have been neglected or simplified, either in order to save computational time, or because their dynamics were considered too fast to be of any interest in a controller synthesis.

3.2. Assumptions

The following assumptions have been made in the development of this model:

- diffusion transients reach immediately their steady-state, and the concentration profile of species is linear with distance from reaction site to bulk;
- the anodic overvoltage is neglected: Ole Edvard Kongstein contributed some measurements to confirm this assumption;
- transients are instantaneous also for the concentration of species in amorphous phosphoric acid, which depend on the partial pressures of the species at the reaction sites;
- the inverse (anodic) reaction on the cathode is first-order with respect to water vapour;
- the ohmic loss in the cell is linear with current;
- cathodic capacitance is constant;
- crossover current is constant.

3.3. Diffusion

A preliminary analysis was run to establish the influence of diffusion transients on the response of fuel cells. Using actual data and formulae as reported by Ceraolo et al. [1], a PBI fuel-cell cathode's reaction surface was modelled, with tortuosity $\xi = 7$, porosity $\varepsilon = 40\%$, distance from reaction site to bulk $L = 0.3$ mm, at a temperature of $T = 150\,^{\circ}\mathrm{C}$. These parameter values are believed to be severe enough to produce a worst-case estimate of the time constant of the diffusion transient. The diffusion process involved water vapour, oxygen and nitrogen, and was modelled with Stefan–Maxwell's equations, in the following form:

$$\frac{\varepsilon}{\xi^2}\frac{\partial p_i}{\partial x} = \sum_{k=1}^{3} \frac{RT}{pD_{ik}}(p_i N_k - p_k N_i) \tag{1}$$

Since diffusion transients are caused by the reaction current density i_r, they will not in any case be faster than i_r's. If the diffusion dynamics is shown to be faster than the one associated with i_r, assuming instantaneous transients for diffusion is an acceptable approximation.

Furthermore, the diffusion transient can have a noticeable effect on the reaction rate only if the partial pressures at the reaction sites are sufficiently low, that is, when the cell is close to the mass-transfer barrier.

It will be assumed in the following that diffusion transients settle immediately, and that all partial-pressure profiles are linear from bulk to reaction site. We can then easily integrate:

$$p_i(x) \simeq p_{i,\mathrm{r}} + \frac{\partial p_i}{\partial x} x \tag{2}$$

Since the Stefan–Maxwell multicomponent diffusion Eq. (1) is valid for any positive distance $x \leq L$ from the reaction site, we can evaluate it with the bulk values of partial pressures, $p_{i,\mathrm{b}} = p_i(L)$, which are known; furthermore, since we neglect the diffusion transient, we can assume that the flows of oxygen, nitrogen and water will be constant in x and directly related to the reaction current i_r:

$$N_{\mathrm{O_2}} = -\frac{i_\mathrm{r}}{4F} \tag{3}$$

$$N_{\mathrm{H_2O}} = \frac{i_\mathrm{r}}{2F} \tag{4}$$

$$N_{\mathrm{N_2}} = 0 \tag{5}$$

Inserting this in the Stefan–Maxwell equations (1) and (2), the resulting direct formulae are

$$p_{\mathrm{O_2,r}} = p_{\mathrm{O_2,b}} - \frac{L\xi^2}{\varepsilon}\frac{RT}{4F}\left(\frac{2p_{\mathrm{O_2,b}} + p_{\mathrm{H_2O,b}}}{pD_{\mathrm{O_2,H_2O}}} + \frac{p_{\mathrm{N_2,b}}}{pD_{\mathrm{O_2,N_2}}}\right) i_\mathrm{r} \tag{6}$$

$$p_{\mathrm{H_2O,r}} = p_{\mathrm{H_2O,b}} + \frac{L\xi^2}{\varepsilon}\frac{RT}{4F}\left(\frac{2p_{\mathrm{O_2,b}} + p_{\mathrm{H_2O,b}}}{pD_{\mathrm{O_2,H_2O}}} + 2\frac{p_{\mathrm{N_2,b}}}{pD_{\mathrm{H_2O,N_2}}}\right) i_\mathrm{r} \tag{7}$$

It can be seen that, in this approximation, the reaction-site partial pressures vary linearly with reaction-current density. Incidentally, we can obtain an approximate expression of the current i_L at the mass-transfer limit, which occurs when $p_{\mathrm{O_2,r}} \to 0$, by rearranging Eq. (6):

$$i_\mathrm{L} = p_{\mathrm{O_2,b}}\frac{\varepsilon}{L\xi^2}\frac{4F}{RT}\left(\frac{2p_{\mathrm{O_2,b}} + p_{\mathrm{H_2O,b}}}{pD_{\mathrm{O_2,H_2O}}} + \frac{p_{\mathrm{N_2,b}}}{pD_{\mathrm{O_2,N_2}}}\right)^{-1} \tag{8}$$

While this expression is not an exact one, it is very useful as a rough, inexpensive estimate, and as a first guess in more detailed, iterative solution algorithms.

In Eqs. (6)–(8) the group $\frac{L\xi^2}{\varepsilon}$ appears always together. It is not possible to estimate L, ξ and ε separately in this model, so they will be integrated in a new variable, $\lambda = \frac{L\xi^2}{\varepsilon}$. λ represents the thickness of an equivalent diffusion layer that would result in the same reaction-site partial pressures as in the porous electrode.

3.4. Steady-state activation overvoltage

The model neglects any overvoltages on the anode. Unless differently specified, it will be understood from now on that all electrochemical terms refer to the cathode.

At steady-state, the reaction current density i_r is equal to the circuit current density i plus the crossover current density i_c; i_r represents the reaction rate resulting from the Butler–Volmer equation, i the actual current flowing in the external circuit divided by the cell's area, and i_c the internal losses such as permeation of reactants through the membrane or electronic conductivity of the membrane.

Liu et al. [30] have recently studied the oxygen reduction reaction at the cathode of a PBI fuel cell. Their results (published while this paper was in peer review and subsequently implemented) indicate that the rate-determining step is first-order with respect to oxygen and protons:

$$\mathrm{O_2} + \mathrm{H^+} + \mathrm{e^-} \to \mathrm{O_2H} \tag{9}$$

The remaining steps from $\mathrm{O_2H}$ to $\mathrm{H_2O}$ are faster, and can be assumed to be instantaneous. The oxygen term is the oxygen present in amorphous $\mathrm{H_3PO_4}$, and the concentration of protons can be promoted by water:

$$\mathrm{H_3PO_4} + \mathrm{H_2O} \leftrightarrows \mathrm{H_2PO_4^-} + \mathrm{H_3O^+} \tag{10}$$

In the data range of interest, the data provided by Liu et al. seems to indicate that the concentration of $\mathrm{H^+}$ is approximately proportional to the partial pressure of water vapour.

There are no equivalent studies for the inverse reaction of water oxidation, so it will be simply assumed to be first-order with respect to water:

$$\tfrac{1}{2}\mathrm{H_2O} \to \mathrm{H^+} + \mathrm{e^-} + \tfrac{1}{4}\mathrm{O_2} \tag{11}$$

Assuming that the activity of oxygen in the amorphous $\mathrm{H_3PO_4}$ phase is proportional to the partial pressure of oxygen at the reaction site (with no or negligibly fast transient), the following expression results for the exchange current density [31]:

$$i_0 = nFk\left(\frac{p_{\mathrm{O_2}}}{p_0}\right)^{\alpha}\left(\frac{p_{\mathrm{H_2O}}}{p_0}\right)^{(1+\alpha)/2} \tag{12}$$

where n is equal to 1 and p_0 is the standard pressure (101 325 Pa). Finally, Liu et al. also provided an estimate for the symmetry factor α, in the range 0.42–0.44; $\alpha = 0.43$ will be assumed.

Then, the activation overvoltage η can be calculated for a given current, according to the Butler–Volmer equation:

$$i_\mathrm{r} = i_0(\mathrm{e}^{\alpha(nF/RT)\eta} - \mathrm{e}^{-(1-\alpha)(nF/RT)\eta}) \tag{13}$$

Since this equation, which binds η and the reaction current density i_r, cannot be explicitly inverted and expressed directly as a function of type $\eta = f(i_\mathrm{r})$, an iterative algorithm is necessary.

At this point, η is known, and there remains only to calculate the reversible cell potential E^{rev}, which can be found from well-known thermodynamic data:

$$E^{\mathrm{rev}} = \frac{-\Delta g_f}{nF} \tag{14}$$

Δg_f is calculated using the partial pressures at the reaction sites. The ohmic loss is easily found as $r_{\mathrm{cell}}(i + i_\mathrm{c})$. The cell voltage is then found as

$$V = E^{\mathrm{rev}} - \eta - r_{\mathrm{cell}}(i + i_\mathrm{c}) \tag{15}$$

r_{cell} is here assumed to be constant.

3.5. Dynamics

During transients the reaction current density i_r is different from the sum of current density (due to the external load) and crossover current density (due to losses). Looking at the following differential Eq. (1), it is clear that the difference $i + i_c - i_r$ is actually the driving force of the transient behaviour of the activation overvoltage:

$$\dot{\eta} = \frac{i + i_c - i_r}{C} \tag{16}$$

This is the only differential equation that we consider in order to compute the transient of the fuel cell. As already mentioned, all diffusion transients will be neglected; any capacitance or inductance in any part of the load is also neglected. Capacitance C is assumed to be constant; however, in real-world operation, C varies: in PEM fuel cells, a variation of capacitance as a function of cell potential has been investigated, for example, by Parthasarathy et al. [32].

The load in the model is generally allowed to vary with time, and is described by a function of the form $I = f(V, t)$. It has been chosen to use this form instead of $V = g(I, t)$ because current I through MOSFETs flattens out beyond a certain value of the source-drain voltage V (depending on the MOSFETs gate voltage), and this yields an infinite number of values of V for a single value of I. MOSFETs are interesting candidates as control actuators in linear control, and therefore it is considered important that the model be able to simulate them.

The differential Eq. (16) describing the activation overvoltage looks simple: i is the actual current in the circuit, whereas i_r is the *reaction current*, or the current that corresponds to the consumption of reactants in the fuel cell. The crossover current i_c represents current that is generated, but is lost inside the fuel cell. The net sum of these quantities is the rate of accumulation of charge in the model's capacitor, which represents the sum of an electrostatic double layer capacitance, a *pseudocapacitance* due to charge stored by adsorbed and intermediate products at the surface, and the charge stored in the diffusion layers [33]. Divided by the capacity C, this sum yields the time derivative of the cathodic activation overvoltage, $\dot{\eta}$.

The model can be expressed in a diagram, as shown in Fig. 2. There, one can see the internal resistance r_{cell}, the reversible potential E^{rev}, the capacitor C and its overvoltage η. The bipole in parallel with the capacitor is a nonlinear voltage-controlled current generator, which enforces the Butler–Volmer law imposing a current i_r as a function of η (and many other parameters, as per Eq. (13)). This bipole is often also modelled as a nonlinear resistance [34], or a linearised value in an area of interest. Incidentally, the ideal generator E^{rev} and the resistance r_{cell} in series with it can be viewed as a Thevenin equivalent circuit.

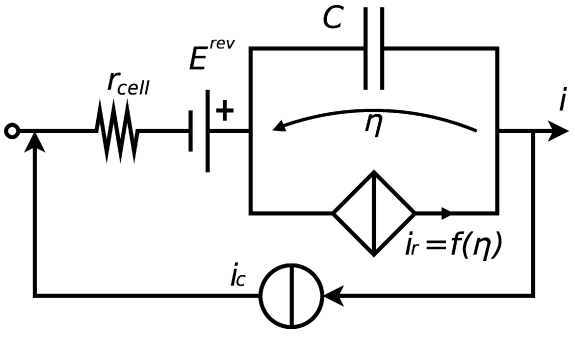

Fig. 2. Diagram of the fuel-cell model.

Table 1
Summary of the main equations used in the model

Overvoltage differential equation	$\dot{\eta} = \frac{i+i_c-i_r}{C}$	
Butler–Volmer equation	$i_r = i_0 \left(e^{\alpha(nF/RT)\eta} - e^{-(1-\alpha)(nF/RT)\eta}\right)$	
Exchange current density	$i_0 = nFk \left(\frac{p_{O_2,r}}{p_0}\right)^{\alpha} \left(\frac{p_{H_2O,r}}{p_0}\right)^{(1+\alpha)/2}$	(12')
Oxygen diffusion	$p_{O_2,r} = f(i_r, p_{i,b}, \lambda, T)$	(6')
Water diffusion	$p_{H_2O,r} = g(i_r, p_{i,b}, \lambda, T)$	(7')

The actual integration of Eq. (16) is not very simple, since i_r is a function of many parameters, including η itself, through the Butler–Volmer equation (13). Furthermore, the exchange current density i_0 in that equation depends on the reaction-site concentrations of the reactants (Eq. (12)), which, in turn, depend on their consumption rate, proportional to i_r. An iterative loop, consisting of Eqs. (6), (7), (12) and (13), is therefore necessary to calculate i_r at all integration steps, and this is the major computational cost of the simulation. This phenomenon could be approximated assuming a constant i_0, but a separate, empirical term for mass-transport overvoltage should then be introduced in Eq. (15). The complete set of equations to solve is summarized in Table 1.

The overall function that calculates the transient simulation, based on the selected time steps and the external load's function, calculates first the initial state of the fuel cell, which is represented by its activation overvoltage η_0. To find it, the model assumes that the system is initially at steady-state.

3.6. Time constants

Given the state x of a dynamic system, a time constant is the factor τ in the following differential equation:

$$\tau \dot{x} = -x \tag{17}$$

In this equation forcing terms were neglected for sake of simplicity. We will now show how to obtain a simple relationship for the time constant of the electrochemical transient of fuel cells.

The external characteristic is assumed to be a generally nonlinear, purely resistive load of the type $V = \Psi(i)$. The reversible voltage E^{rev}, the cell's internal resistance r_{cell} and the crossover current i_c are assumed to be constant. The time derivative of the cell's voltage is then expressed as

$$\frac{dV}{dt} = \frac{d}{dt}[E^{rev} - \eta - r_{cell}(i + i_c)] = -\frac{d}{dt}(\eta + r_{cell} i) \tag{18}$$

Since the operating point has to be on the load's characteristic as well as on the cell's instantaneous one, it can be written that

$$\frac{dV}{dt} = \frac{d\Psi}{dt} = \left.\frac{d\Psi}{di}\right|_i \frac{di}{dt} \tag{19}$$

Inserting in Eq. (18) and rearranging

$$\frac{di}{dt} = -\left(r_{cell} + \left.\frac{d\Psi}{di}\right|_i\right)^{-1} \frac{d\eta}{dt}$$

$$= -\left(r_{cell} + \left.\frac{d\Psi}{di}\right|_i\right)^{-1} \frac{i + i_c - i_r}{C} \quad (20)$$

The overvoltage's time derivative is

$$\frac{d\eta}{dt} = \frac{i + i_c - i_r}{C} = \left.\frac{d\eta}{di_r}\right|_{i_r} \frac{di_r}{dt} \quad (21)$$

Rearranging:

$$\frac{di_r}{dt} = \left(\left.\frac{d\eta}{di_r}\right|_{i_r}\right)^{-1} \frac{i + i_c - i_r}{C} \quad (22)$$

Subtracting Eq. (22) from Eq. (20), we obtain the following relationship:

$$\frac{d(i + i_c - i_r)}{dt} = -\underbrace{\frac{1}{C}\left[\left(r_{cell} + \left.\frac{d\Psi}{di}\right|_i\right)^{-1} + \left(\left.\frac{d\eta}{di_r}\right|_{i_r}\right)^{-1}\right]}_{1/\tau} \times (i + i_c - i_r) \quad (23)$$

Assuming that C and r_{cell} are constant, that functions $\Psi(i)$ and $\eta(i_r, \ldots)$ are given, the time "constant" τ depends essentially on i and i_r:

$$\tau(i, i_r) = \frac{C}{\left(r_{cell} + \left.\frac{d\Psi}{di}\right|_i\right)^{-1} + \left(\left.\frac{d\eta}{di_r}\right|_{i_r}\right)^{-1}} \quad (24)$$

The reasons for using $i + i_c - i_r$, which represents the current inflow in the capacitor and is therefore proportional to the time derivative of the overvoltage η, as a state of the system, instead of the more natural η itself, are that it is possible to find expression (23) explicitly, without solving numerically the Butler–Volmer equation (13), and that it is not necessary to add a forcing term to account for external effects, since they are already included through Ψ; furthermore, the term $i + i_c - i_r$ always returns to 0 at the end of a transient, since it is the transient's driving force.

4. Results and discussion

4.1. Polarisation curve

The polarisation curve obtained at the conditions described in the previous section is shown in Fig. 3. It can be seen that the polarisation curve shows a fairly large hysteresis. This behaviour has been observed previously in other experiments on similar PBI cells in Liu et al. [30].

Since Liu et al. showed that the cathodic reaction is first-order with respect to the concentration of H^+ ions, which depends on the partial pressure of water vapour, it might be tempting to blame the hysteresis on the lag in the formation of water.

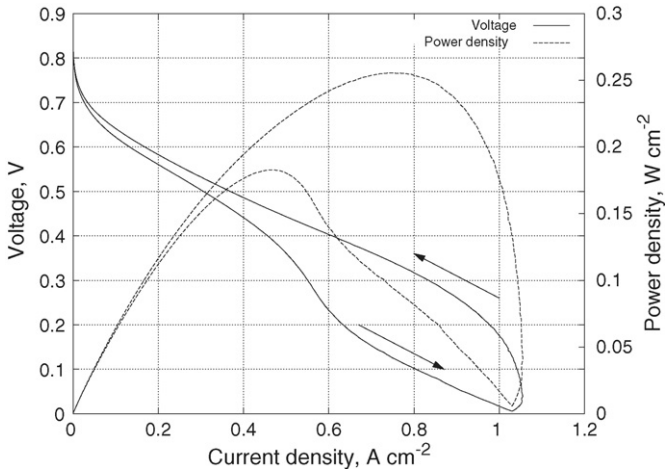

Fig. 3. Experimental polarisation curve of a PBI fuel cell at 150 °C, measured with a sweep rate of 25 μV s^{-1}. The arrows indicate the direction of the hysteresis cycle.

However, given how slowly the polarisation curve was sampled, this is unlikely to be the only reason. Likewise, temperature transients, caused by the varying power output, should not have influenced such a slow sampling. Other possible causes include changes in the access of oxygen to the reaction site or changes in the catalyst during the cycle.

4.2. Anodic overvoltage

The anodic overpotential at 1 A cm^{-2} was measured to be 40 mV, indicating a small anodic overpotential compared to the cathodic one. This justifies the assumption of neglecting the anodic overpotential.

4.3. Resistance steps

The results obtained by switching from an initial resistance to a smaller one and back are shown in Figs. 4 and 5. It can

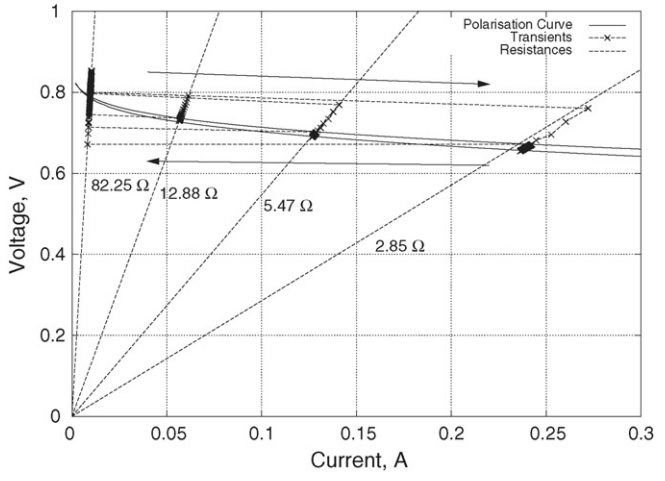

Fig. 4. Experimental operating points' path in the *V–I* diagram after step changes in the external circuit's resistance, starting from 82.25 Ω and switching back. The arrows indicate the path in the *I–V* plan.

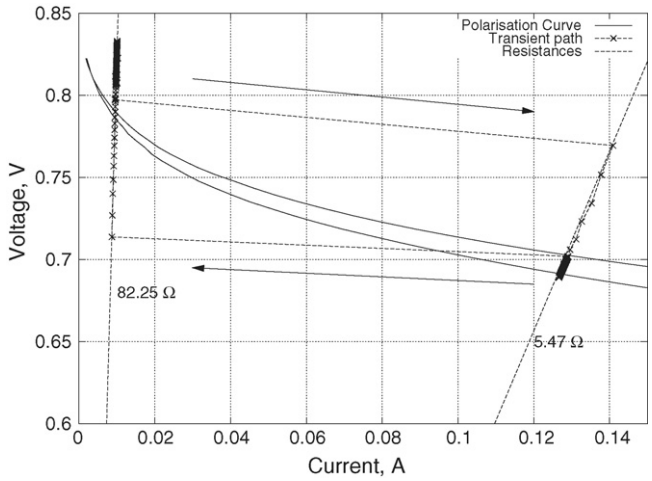

Fig. 5. Zoom on an experimental transient path for a step change in the circuit resistance.

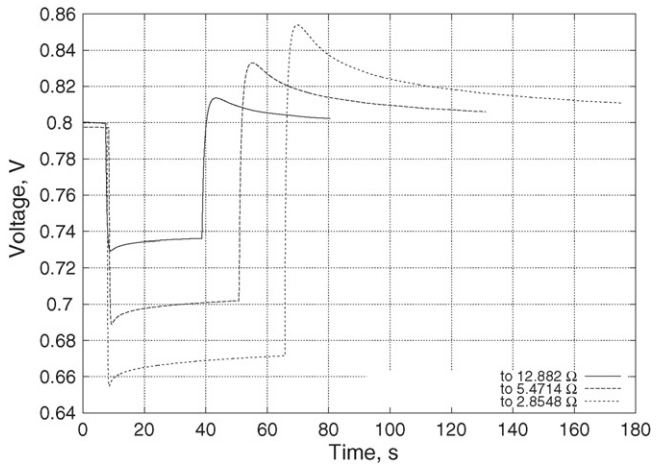

Fig. 6. Experimental voltage transients after the step changes in the external circuit's resistance, starting from 82.25 Ω and switching back.

be seen how the operating point moves from one resistance's characteristic to the other along almost parallel, straight lines. The reason why the lines are not exactly parallel might be that sampling is not continuous, and the operating point might have moved from the initial point on the new characteristic by the time a new sample is measured.

As a reference, the steady-state characteristic is plotted as well. The last transient is not exactly on the expected characteristic of its external resistance, most likely due to imprecision in the calculation of the resistance value.

It is clear that some transients are faster than others in the descent to steady-state; this can be seen by the number of markers, roughly spaced by 0.06 s, on the trajectories in the *V–I* plane. It appears that the electrochemical transient was faster the lower the resistance.

Zooming in on a specific transient provides further information. In Fig. 5 the second transient, the one to 5.47 Ω, is represented in the *V–I* plane; the marks on the line represent the sampling points. It can easily be seen that the descent to steady-state on the characteristic of the 5.47 Ω resistance was faster than the ascent to steady-state on the 82.25 Ω characteristic when the switch on the resistance board was turned off.

There is an indication, in other words, that the electrochemical transient can exhibit different time constants depending on both the start and the end point. This behaviour could be related to the phenomenon observed by Johansen [22], where the same proportional controller performed too aggressively in some operating ranges, and too mildly in others.

The values assumed by the voltage are plotted versus time in Fig. 6. The experiment is the same as in Fig. 4. It can be seen that, after a transient in the order of magnitude of 1 s, a slower transient of generally smaller amplitude appears.

Wang and Wang [35] measured a similar behaviour for a low-temperature PEM fuel cell, which had also been described by Ceraolo et al. [1]. In both cases, the authors noted that slow transients in proton concentration are the cause of these transients. Since protons in the amorphous H_3PO_4 phase are important in PBI fuel cells too [30], the mechanism could be similar in principle. Compared to Wang and Wang's measurements, transients in PBI fuel cells appear to be slower.

It can be seen from Figs. 4 and 5 that all the transients to lower values of resistance seem to reach first the lower branch of the polarisation curve, to rise again to the upper one as proton concentration increases. The transients back to the larger resistance, however, are much larger than the gap between the branches of the polarisation curve; they have larger overshoots for transients arriving from higher values of current, possibly because of higher concentration of protons. This would seem to strengthen the case for a role of water in the hysteresis of the polarisation curve of Fig. 3, but, on the other hand, these transients are much faster (in the order of 10 s) than the sampling rate of the polarisation curve, which would have had enough time to reach the steady-state.

These slower transients are not considered to be an important issue, since in a control-oriented perspective, these secondary transients can easily be controlled by a simple PI feedback controller [36]. Therefore, we shall turn our attention to the first moments of the transient.

4.4. Effect of flow disturbances

It was noted that just changing the oxygen flow rate would change the open-circuit voltage significantly, as shown in Fig. 7. It was initially supposed that variations in temperature could be the cause of this behaviour: in the experimental setup sketched in Fig. 1, gases enter the cell at ambient temperature, and could have cooled the cathode to a temperature lower than that measured by the thermocouple. However, subsequent experiments with gas pre-heating showed that the difference was minimal.

The anode turned out to be less sensitive to inlet hydrogen flow. In fact, changing the hydrogen flow would not cause any measurable disturbance to the operating point.

It can be supposed that variations in proton concentration at the cathode are the cause of these transients too. When oxygen flow is increased, there is an immediate increase in voltage due to higher oxygen partial pressure, and a subsequent decrease due to reduction in proton concentration, caused by the reduced

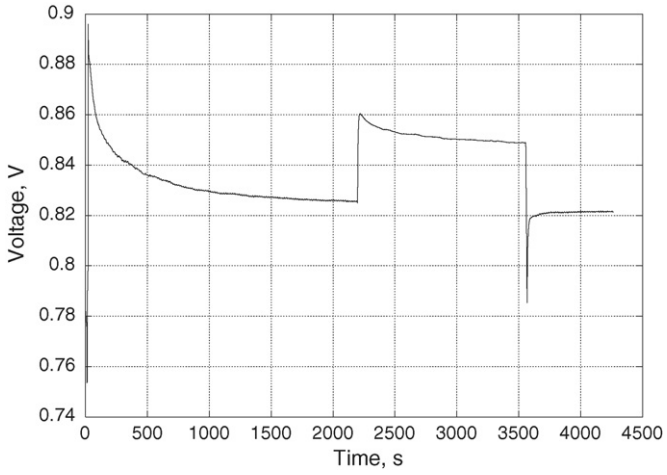

Fig. 7. Experimental measure of the effect of a step in oxygen flow from 3.7 to 18 $cm^3\ s^{-1}$ at 150 °C on open-circuit voltage. The first step is the moment the oxygen flow is started at the beginning of the experiment. The second step, at about $t = 2200$ s, is the moment oxygen flow is stepped up; the last step, at about $t = 3600$ s, is when oxygen flow is stepped back down.

water partial pressure at the reaction site.[2] Conversely, when oxygen flow is reduced, there is a sharp reduction in voltage due to lower oxygen partial pressure, followed by a (this time faster) recovery of proton concentration.

This asymmetry in the dynamics of proton concentration has already been noted in Ceraolo et al. [1].

5. Modelling results and discussion

5.1. Diffusion modelling

The result of diffusion modelling is shown in Fig. 8. This model predicts transients, without overshoots, in the order of 10^{-1} s in case of steps in the reaction rate. Such steps are impossible in reality, since i_r varies continuously as a function of η. As long as the time constants of the transients of i_r are larger than 10^{-1} s, the diffusion transients may safely be assumed instantaneous; they may however be more important where transients in i_r are faster.

Since we have seen that transients usually take longer than this to complete, it is safe to neglect diffusion dynamics. However, this is only valid as long as transients in overvoltage are not faster than the ones in diffusion.

5.2. Model performance

The model, implemented in C++, can calculate a resistance-step transient in a few seconds of computation time on a 2.4 GHz Pentium4 computer under Linux. Previous experience with languages such as Scilab required about 1 min for the same transients, with more marked difficulties when integrating close to the mass-transfer limit.

[2] Even if we are at open circuit, crossover current is causing some reaction to take place, and some water to be formed.

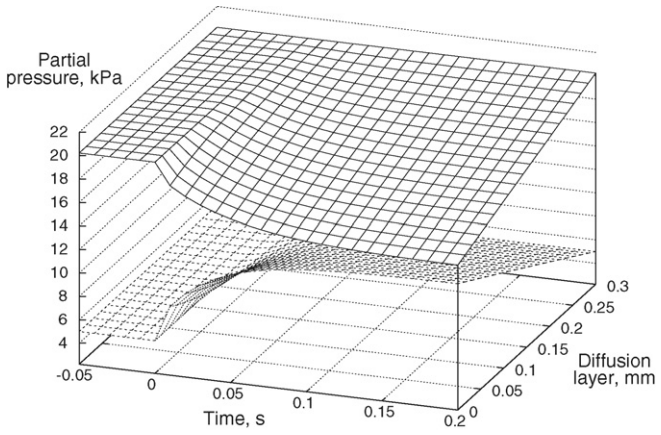

Fig. 8. Simulated concentration transient on the cathode of a PBI fuel cell; the current steps from 0 to 800 A m^{-2} at $t = 0$. The upper profile is oxygen, the lower water vapour.

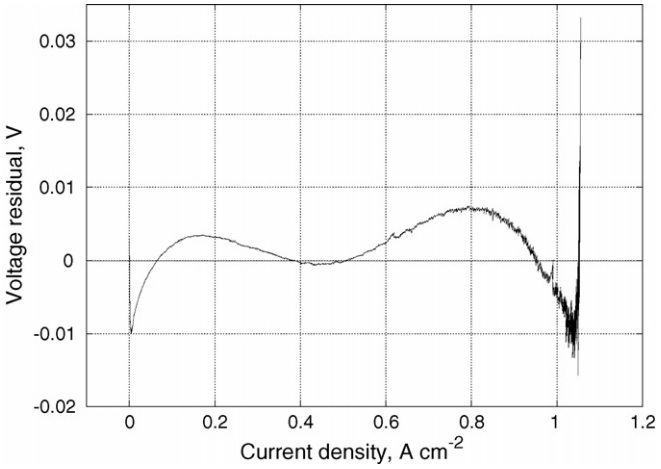

Fig. 9. Plot of residuals (sample minus model values) for the model applied to the upper branch of the polarisation curve shown in Fig. 3.

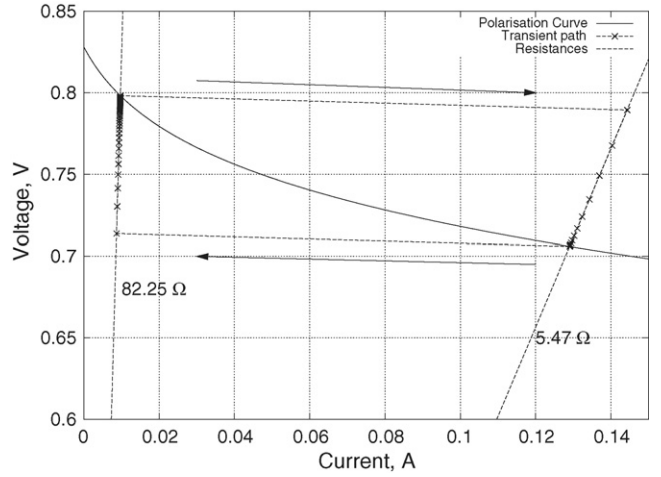

Fig. 10. Simulated transient trying to replicate the experiment in Fig. 5. The value assumed for the capacitance is 1500 F m^{-2}. The markers are spaced by 0.06 s, except those at switching points that are spaced 1 μs.

Table 2
The results of the parameter regression for parameters k, i_c, λ and r_{cell} with the data of the upper branch of the polarisation curve presented in Fig. 3

	Estimate	$\pm\sigma$	Units	Correlation matrix			
k	115.7	55.9	$\mu mol\,m^{-2}\,s^{-1}$	1	−0.590	0.672	0.847
λ	25.82	0.349	mm	−0.590	1	−0.740	−0.648
i_c	33.63	93.94	$A\,m^{-2}$	0.672	−0.740	1	0.518
r_{cell}	26.07	5.96	$\mu\,\Omega\,m^2$	0.847	−0.648	0.518	1

5.3. Parameter regression

A parameter regression has been carried out to verify whether and how well the proposed model fits the results. We were initially sceptical about a parameter regression to find k and other parameters, because of the large hysteresis of the polarisation curve in Fig. 3: however, we noticed the model fits very well the upper branch of the curve, and were able to regress to some satisfactory parameter values and produce a residual plot. However, the lower branch does not qualitatively fit even with different values.

The residuals are plotted in Fig. 9, where it can be seen that the model predicts the cell's voltage in the upper branch with an approximation of ± 10 mV until it reaches the mass-transport limit. The results of the parameter regression are shown in Table 2. Estimates, standard deviations, units and the parameters' correlation matrix are given.

There is significant correlation between internal resistance r_{cell} and the reaction constant k, since in most experimental points the effect of increased resistance is similar to that of a reduced reaction constant. Similarly, there is high correlation between crossover current density i_c and the effective thickness of the diffusion layer λ: since information on λ is gathered mostly at data points close to the mass-transport barrier, if i_c is larger, λ must be thinner, to allow more reaction current ($i_r = i + i_c$) to pass at the mass-transport limit in order to result in the same measured values of i. To reduce these correlations, one may gather data points from conditions where the effects of these parameters are going to vary independently, such as different values of temperature or gas composition.

The model does not fit the lower branch of the polarisation curve. It is possible that the lower branch follows different kinetics, or other factors, such as catalyst deactivation and transients in proton concentration, interfered in the measurement and caused the hysteresis observable in the slow scan (Fig. 3).

Some computational difficulties were experienced as the regression algorithm could sometimes converge to a local minimum different from the global one.

It was not possible to perform a proper parameter estimation for the cathodic capacitance, as the slower secondary transients shown in Fig. 6 are not well understood, and would have interfered in the regression procedure. Furthermore, the exact time of switching could not be logged in the measurements. However, a value in the range of 1–2k $F\,m^{-2}$ seems to reproduce the observed behaviour with acceptable approximation. The value $1500\,F\,m^{-2}$ has been used in Fig. 10.

5.4. Path on the V–I diagram

The cause of the sudden iso-η "kick" in the dynamic path diagram, as can be seen in the simulation in Fig. 10 and in experimental results in Figs. 4 and 5, is caused by the simple fact that the operating point must always lie on the load's characteristic, when the load is purely resistive. It is possible to determine to *which coordinates* on the load's characteristic the operating point will jump, considering that the activation overvoltage η varies continuously with time; when a step change in the outer load happens at time t_0, η will be the same for times t_0^+ and t_0^-.

For every point in the steady-state polarisation curve we can identify its iso-η line, which represents the set of operating points to which the fuel cell can jump instantaneously. This line is the characteristic of the cell's internal resistance. The equation is the same as Eq. (15), but the first two terms (E^{rev} and η) are now constant for each instantaneous characteristic, since they depend on i_r.

$$V(i) = \underbrace{E^{rev} - \eta}_{\text{constant}} - r_{cell}(i + i_c) \tag{25}$$

We can visualise this line as a sort of *time-varying characteristic*: when the external load changes, the operating point moves immediately to the new intersection between the new load's characteristic and the iso-η line (the instantaneous characteristic). As the value of i will change accordingly, $i + i_c - i_r$ will no longer be equal to zero, and this will cause the overvoltage η to vary with time according to differential Eq. (16). This means that the iso-η line will start moving vertically according to the characteristic Eq. (25), until the intersection between it and the load's characteristic is again on the steady-state polarisation curve, where by definition $i + i_c \equiv i_r$.

Using the load characteristic as the model's input has allowed to simulate real laboratory results, and has given the possibility of simulating the implementation of MOSFETs as manipulated variables in control of fuel cells. MOSFET transistors are loads whose characteristic can be changed by manipulating a *gate voltage*. The load's current enters from a source, and exits from a drain; the gate is a third connection point, whose voltage compared to the source is the manipulated variable; since no net current flows from the gate to either source or drain, little or no power is consumed by the process of changing the MOSFET's characteristic. MOSFETs can be imagined as fail-closed fluid-flow valves: when no gate voltage is applied, no current may pass. As the gate voltage increases beyond a certain threshold, the characteristic detaches from the open-circuit's and allows more current to pass. Normally, for every gate voltage there is a maximum current that can pass through the MOSFET, regardless of the voltage across the source and drain of the transistor.

More details on transistors and MOSFETs in particular can be found in textbooks such as Mohan et al. [37].

The simulation of a MOSFET's gate-voltage step is illustrated in Fig. 11. The MOSFET was modelled according to a data sheet for a IRF1404 power MOSFET provided by International Rectifier, Inc.

5.5. Effects of parameters on the dynamics

Examining Eq. (24), it is possible to understand the influence of some parameters on the dynamic response of a fuel cell.

The time constants are directly proportional to the electrode capacitance C. As this capacitance may vary [32], the time constants may vary accordingly: the larger the capacitance, the slower the transient.

The denominator of Eq. (24) is made up of two terms. When both are small, the transient will be slower; if, instead, one or both terms in the denominator are large, the dynamics will be faster. This means that the time constants will be sensibly larger when there is a large sum of internal and external resistances and a large variation of the overvoltage with reaction current. Conversely, if any of these two is small, the time constants will be smaller. This is consistent with the observation of faster transients at high values of current, as in Figs. 4 and 5.

The time constants can also be interpreted graphically. In Fig. 5 it was observed that the electrochemical transients that occurred when stepping the value of the outer circuit's resistance varied in duration depending on the direction of the step. This has been confirmed by the model in Fig. 10. It is possible to visualise the cause of this behaviour by means of the instantaneous characteristic, or iso-η line, that was previously introduced.

The transient's differential Eq. (16) states that $\dot{\eta} \propto (i + i_c - i_r)$. It is therefore important to be able to visualise the position of i and i_r on the plot during the transient. As long as the load is purely resistive, the operating point is bound to be on the external circuit characteristic. However, it must also be on one of the feasible points for the fuel cell, which are represented by the instantaneous characteristic: therefore, the current density i always lies at the intersection between the load's characteristic and the cell's instantaneous characteristic.

i_r is the reaction current density corresponding to overvoltage η; at any time, it represents the rate of the electrochemical reaction. The instantaneous characteristic represents all the operating points to which the fuel cell can be moved instantly; its intersection with the steady-state polarisation curve represents therefore the steady-state point corresponding to the present value of the overvoltage η, and is at the coordinate $i_r - i_c$ on the i axis.

Therefore, i is found at the intersection of the instantaneous characteristic with the external load, and $i_r - i_c$ at the intersection of the instantaneous characteristic with the polarisation curve.

Looking at the simulated transient in Fig. 10, it is clear that the drawn part of the polarisation curve is closer to the characteristic of the higher resistance, when distance is measured along the i axis. Since $\dot{\eta}$ is proportional to the distance between the intersections of the instantaneous characteristic with the polarisation curve and the external resistance along the i axis, i.e. $i + i_c - i_r$, it follows immediately that the transient to the lower resistance will be faster than the one coming back, because of the higher values of $i + i_c - i_r$ along that path; this is confirmed by the experimental measurements shown in Figs. 4 and 5.

5.6. Conditions for perfect power control

Considering the basic expression of the voltage of a fuel cell (15), and looking at Fig. 10, it is evident that the instantaneous characteristic at a given steady-state point stays at higher voltages than the polarisation curve when moving to higher values of current density, and, conversely, at lower voltages for lower values of current density. This happens because the instantaneous characteristic is representative of a single value of η, which is strictly increasing with current density. This results in power overshoots in any transient that starts and ends in a range of currents lower than the one associated to the maximum power output, which is often close to the mass-transfer limiting current

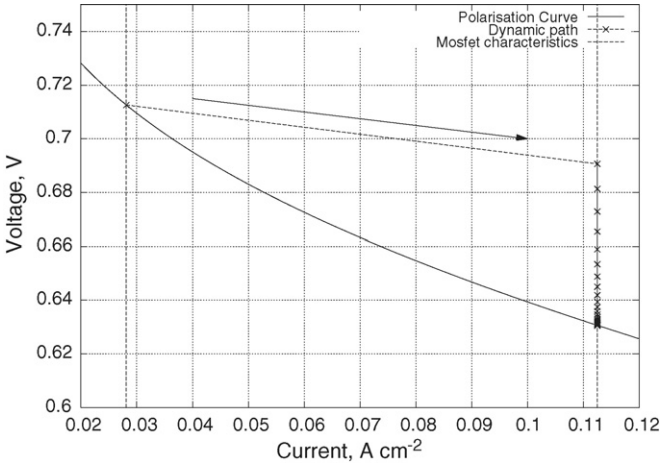

Fig. 11. The simulated transient resulting from having changed the gate voltage of a MOSFET from 3.05 to 3.1 V, when this MOSFET is operating as the load of a PBI fuel cell at 150 °C. The markers are spaced by 0.01 s, except for the switching instant when there is a spacing of 1 μs.

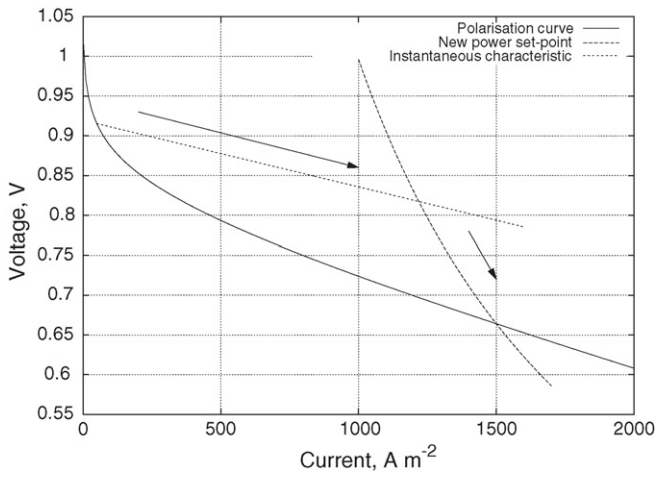

Fig. 12. A perfect response to a step in the set-point for power might be obtained moving the operating point to the intersection of the iso-η curve with the iso-power curve, and following the iso-power curve until steady-state is achieved.

i_L; it is normal to assume that the cell will operate below this current density, as operating above it results in inefficient and undesirable operation.

Under these assumptions, a perfect step change in power output can be obtained by leading the operating point to the intersection between the instantaneous characteristic and the iso-power line of the new power output; this intersection always exists if the new power reference is less than or equal to the maximum power that the cell can produce at steady-state. Then, by continuously adjusting the external characteristic (possibly with a feedback-controlled MOSFET), the operating point can be led along a constant-power line, until it finally intersects the polarisation curve, where the transient will stop. Fig. 12 shows how such a transient should look like.

6. Conclusion

A steady-state model of a PBI fuel cell was developed, and its parameters were estimated by means of parameter regression on experimental data. However, the model fits well only one branch of the polarisation curve, which presented significant hysteresis. The cause of this hysteresis is not well understood.

A pattern was identified in transient tests of the same cell when changing the resistance of the load. Neglecting the slower dynamics, a dynamic model based on the Butler–Volmer equation has been developed for the overvoltage transient. The novelty in this model is the use of a function, the external load characteristic, as input, rather than the more common approach of using current or voltage. The model also allows to use of MOSFETs, and any other devices with varying characteristic. Usage of current or voltage as an input would have been unfortunate, as neither can be a manipulated variable in a control system.

This new approach allowed to explain the observed transient paths in a simple way, identifying the activation overvoltage η as a state of the fuel cell, together with temperature and compositions. The model was also able to simulate the different dynamics observed when switching back and forth between two external resistances. A simple formula to estimate the time constants of the dynamics has been developed, which allows to predict an approximate value for the transient's time constant τ for an operating point.

Finally, it was shown how a step in the set-point for power output can in theory be perfectly matched by the power output of the fuel cell, if proper control could be applied, under quite general assumptions on operating conditions.

Acknowledgements

We acknowledge the help we received from Helge Weydahl, who made the variable-resistance board. Steffen Møller-Holst is acknowledged for valuable contributions during scientific discussions and for project management.

This work has received financial support from the Norwegian Research Council, Statoil AS, and the European Commission in the 6th Framework Programme.

References

[1] M. Ceraolo, C. Miulli, A. Pozio, Modelling static and dynamic behaviour of proton exchange membrane fuel cells on the basis of electro-chemical description, J. Power Sources 113 (2003) 131–144.
[2] B.S. Kang, J.-H. Koh, H.C. Lim, Experimental study on the dynamic characteristic of kW-scale molten-carbonate fuel cell-systems, J. Power Sources 94 (2001) 51–62.
[3] C.N. Maxoulis, D.N. Tsinoglou, G.C. Koltsakis, Modeling of automotive fuel cell operation in driving cycles, Energy Convers. Manage. 45 (2004) 559–573.
[4] K. Sundmacher, T. Schultz, S. Zhou, K. Scott, M. Ginkel, E.D. Gilles, Dynamics of the direct methanol fuel cell (DMFC): experiments and model-based analysis, Chem. Eng. Sci. 56 (2001) 333–341.
[5] S. Yerramalla, A. Davari, A. Feliachi, T. Biswas, Modeling and simulation of the dynamic behaviour of a polymer electrolyte membrane fuel cell, J. Power Sources 124 (2003) 104–113.
[6] J.B. Benziger, I.G. Kevrekidis, M.B. Satterfield, W.H.J. Hogarth, J.P. Nehlsen, The power performance curve for engineering analysis of a fuel cell, in: AIChE Annual Meeting, 2005.
[7] H. Weydahl, S. Møller-Holst, T. Burchardt, G. Hagen, Dynamic behaviour of an alkaline fuel cell—results from introductory experiments, in: Proceedings of the First European Hydrogen Energy Conference, Grenoble, 2003 (CP4/123).
[8] R.M. Rao, R. Rengaswamy, Study of dynamic interactions of various phenomena in proton exchange membrane fuel cells (PEMFC) using detailed models for multivariable control, in: AIChE Annual Meeting, 2005.
[9] P. Musto, F.E. Karasz, W.J. MacKnight, Fourier transform infra-red spectroscopy on the thermo-oxidative degradation of polybenzimidazole and of a polybenzimidazole/polyetherimide blend, Polymer 34 (14) (1993) 2394–2945.
[10] S.M. Aharoni, A.J. Signorelli, Electrical resistivity and ESCA studies on neutral poly(alkylbenzimidazoles), their salts, and complexes, J. Appl. Polym. Sci. 23 (1979) 2653–2660.
[11] H.A. Pohl, R.P. Chartoff, Carriers and unpaired spins in some organic semiconductors, J. Polym. Sci. A 2 (1964) 2787–2806.
[12] R. Bouchet, R. Miller, M. Duclot, J.L. Souquet, A thermodynamic approach to proton conductivity in acid-doped polybenzimidazole, Solid State Ionics 145 (2001) 69–78.
[13] H. Pu, W.H. Meyer, G. Wegner, Proton transport in polybenzimidazole with H_3PO_4 or H_2SO_4, J. Polym. Sci. 40 (2002) 663–669.
[14] A. Schechter, R.F. Savinell, Imidazole and 1-methyl imidazole in phosphoric acid doped polybenzimidazole electrolyte for fuel cells, Solid State Ionics 147 (2002) 181–187.
[15] R. He, Q. Li, G. Xiao, N.J. Bjerrum, Proton conductivity of phosphoric acid doped polybenzimidazole and its composites with inorganic proton conductors, J. Membr. Sci. 226 (2003) 169–184.
[16] Y.-L. Ma, J.S. Wainright, M.H. Litt, R.F. Savinell, Conductivity of PBI membranes for high-temperature polymer electrolyte fuel cells, J. Electrochem. Soc. 151 (1) (2004) A8–A16.
[17] J.S. Wainright, J.-T. Wang, D. Weng, R.F. Savinell, M. Litt, Acid-doped polybenzimidazoles: a new polymer electrolyte, J. Electrochem. Soc. 142 (7) (1995) L121–L123.
[18] Q. Li, R. He, J.-A. Gao, J.O. Jensen, N.J. Bjerrum, The CO poisoning effect in PEMFCS operation at temperatures up to 200 °C, J. Electrochem. Soc. 150 (12) (2003) A1599–A1605.
[19] C. Shen, G.-Y. Cao, X.-J. Zhu, X.-J. Sun, Nonlinear modeling and adaptive fuzzy control of MCFC stack, J. Process Control 12 (2002) 831–839.
[20] S. Caux, J. Lachaize, M. Fadel, P. Shott, L. Nicod, Modelling and control of a fuel cell system and storage elements in transport applications, J. Process Control 15 (2005) 481–491.
[21] M.T. Iqbal, Modeling and control of a wind fuel cell hybrid energy system, Renewable energy 28 (2003) 223–237.
[22] R.L. Johansen, Fuel cells in vehicles, Master's Thesis, Norwegian University of Science and Technology, 2003.
[23] J.T. Pukrushpan, Modeling and control of fuel cell systems and fuel processors, PhD Thesis, Department of Mechanical Engineering, University of Michigan, Ann Arbor, MI, USA, 2003.

[24] L. Guzzella, Control oriented modelling of fuel-cell based vehicles, in: Proceedings of the Nsf workshop on the integration of modeling and control for automotive systems, 1999.
[25] H. Weydahl, I.A. Lervik, A.M. Svensson, T. Burchardt, S. Møller-Holst, B. Børresen, G. Hagen, Fundamental studies of the dynamic behaviour of an alkaline fuel cell, in: Proceedings of the 2004 Fuel Cell Seminar in San Antonio, Texas, 2004.
[26] P. Argyropoulos, K. Scott, W.M. Taama, Dynamic response of the direct methanol fuel cell under variable load conditions, J. Power Sources 87 (2000) 153–161.
[27] F. Seland, T. Berning, B. Børresen, R. Tunold, Improving the performance of high-temperature PEM fuel cells based on PBI electrolyte, J. Power Sources, in press.
[28] A. Küver, I. Vogel, W. Vielstich, Distinct performance evaluation of a direct methanol SPE fuel cell. A new method using a dynamic hydrogen reference electrode, J. Power Sources 52 (1994) 77–80.
[29] F. Zenith, H. Weydahl, I.A. Lervik, T. Burchardt, S. Møller-Holst, S. Skogestad, G. Hagen, Modelling and experimental study of the transient response of fuel cells, in: Proceedings of the Ninth Ulm ElectroChemical Talks, 2004, pp. 82–83.
[30] Z. Liu, J.S. Wainright, M.H. Litt, R.F. Savinell, Study of the oxygen reduction reaction (ORR) at Pt interfaced with phosphoric acid doped polybenzimidazole at elevated temperature and low relative humidity, Electrochim. Acta 51 (2006) 3914–3923.
[31] J. Newman, K.E. Thomas-Alyea, Electrochemical Systems, Chapter 8: Models for Electrode Kinetics, 3rd ed., John Wiley & Sons, 2004, pp. 212–213.
[32] A. Parthasarathy, B. Davé, S. Srinivasan, A.J. Appleby, C.R. Martin, The platinum microelectrode/Nafion interface: an electrochemical impedance spectroscopic analysis of oxygen reduction kinetics and Nafion characteristics, J. Electrochem. Soc. 139 (6) (1992) 1634–1641.
[33] J. Newman, K.E. Thomas-Alyea, Electrochemical Systems, 3rd ed., John Wiley & Sons, 2004.
[34] P.R. Pathapati, X. Xue, J. Tang, A new dynamic model for predicting transient phenomena in a PEM fuel cell system, Renewable energy 30 (2005) 1–22.
[35] Y. Wang, C.-Y. Wang, Transient analysis of polymer electrolyte fuel cells, Electrochim. Acta 50 (2005) 1307–1315.
[36] S. Skogestad, Simple analytic rules for model reduction and PID controller tuning, J. Process Control 13 (2003) 291–309.
[37] N. Mohan, T.M. Undeland, W.P. Robbins, Power Electronics: Converters, Applications and Design, 2nd ed., John Wiley & Sons, Inc., 1995.